Digital Full-Band Linearization of Wideband Direct-Conversion Receiver for Radar and Communications Applications

Markus Allén, Jaakko Marttila, and Mikko Valkama
Department of Electronics and Communications Engineering
Tampere University of Technology
P.O. Box 692, FI-33101 Tampere, Finland
{markus.allen, jaakko.marttila, mikko.e.valkama}@tut.fi

Simran Singh, Michael Epp, and Wolfgang Schlecker
Airbus Defence and Space GmbH
Airbus Group
Wörthstrasse 85, D-89077, Ulm, Germany
{simran.singh, michael.epp, wolfgang.schlecker}@airbus.com

***Abstract*—This paper proposes a fully digital post-processing solution for cancelling nonlinear distortion and mirror-frequency interference in wideband direct-conversion receivers (DCRs). Favorable cost, integrability, and power efficiency have made DCRs a popular choice in communication systems. It is also an emerging trend in radar systems since digital post-processing enables sufficient performance. The proposed method cancels the most essential distortion adaptively during normal receiver operation without any prior information. Improved cancellation performance compared to the state-of-the-art is achieved considering inband and neighboring band distortion induced by the strong received signals. This is verified and demonstrated with extensive simulations and true RF hardware measurements.**

***Index Terms*—Direct-conversion receiver, interference cancellation, nonlinearity modeling, nonlinear distortion, radar**

I. Introduction

Direct-conversion receivers (DCRs) have recently become more and more popular in different applications, such as radar and mobile communications. This receiver structure has certain benefits over, e.g., traditional superheterodyne receivers. These are flexibility, cost efficiency and integrability [1], [2]. In phased-array radar systems, several receivers are required, which makes DCRs a desirable choice [3]. In a communications receiver, the number of receiver chains is usually smaller, but on the other hand number of devices in a whole system is high and, especially in the mobile devices, the size and cost of the receiver are limited. These limitations, combined with the strict performance requirements of the applications, create scenarios where the state-of-the-art analog hardware cannot deliver high enough linearity [4], [5]. Modern digital post-processing, however, offers a flexible method for improving the receiver linearity.

For linearizing a DCR and, e.g., recovering the weak communications signal, an adaptive interference cancellation (AIC) algorithm has been recently proposed [6]. The AIC has a known weakness of limited performance on the frequency bands in close proximity of the strong blockers. At the same time, these bands are also the ones that suffer the most distortion. This limitation stems from the same characteristics that rule out also distortion cancellation on the blocker band itself. In addition, if only a single signal is received in a certain frequency band, which is typical especially in the radar applications, the only source of distortion is the signal itself. Although it would be desired to cancel the nonlinear distortion in the signal band, the previously proposed AIC is not able to do that. In the literature, some of the AIC challenges have been circumvented by modeling the distortion in analog domain and digitizing this estimate using an additional receiver branch [7], [8]. However, adding more analog hardware is not feasible in all systems. This would be especially challenging in radars which already require significant amount of parallel receivers.

The full-band adaptive interference cancellation (FB-AIC) method proposed in this paper is a fully digital linearization method which does not need any additional analog hardware. However, it is still able to solve all the aforementioned challenges. In other words, FB-AIC is applicable to both radar and communications receivers and is able to adaptively cancel nonlinear distortion during the normal receiver operation. The cancellation principle is based on exploiting the distortion outside the signal band to learn and adapt nonlinearity model coefficients so that full-band cancellation is achieved.

The remainder of the paper is organized as follows. Section II discusses in detail the nonlinearity challenges in radar and communications receivers. Section III introduces the linearization method proposed in this paper, the FB-AIC. The simulation and RF measurement results illustrating the linearization performance are given in Section IV. Finally, the paper is concluded in Section V.

II. Receiver Nonlinearities in Radar and Communications Systems

Fig. 1 illustrates a conceptual block diagram of a direct-conversion receiver. Components which are essential sources of nonlinearity and in-phase/quadrature (I/Q) mismatch are

This work was supported by Airbus Defence and Space GmbH, Finnish Funding Agency for Technology and Innovation (Tekes) under the project "Enabling Methods for Dynamic Spectrum Access and Cognitive Radio" within TRIAL technology programme, The Academy of Finland under the project 251138 "Digitally-Enhanced RF for Cognitive Radio Devices", and Austrian Competence Center in Mechatronics (ACCM).

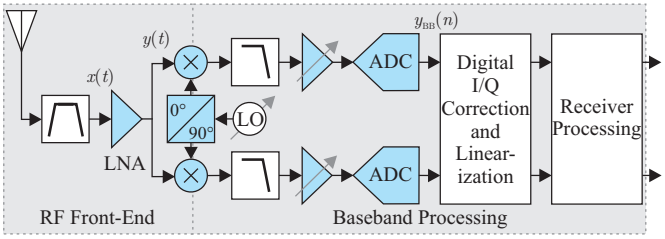

Fig. 1. Conceptual direct-conversion receiver block diagram emphasizing the main sources of nonlinearity and I/Q mismatch together with the employed baseband equivalent mathematical notation.

highlighted. RF, mixing, and baseband (BB) stages are cascaded in reality and therefore proper nonlinearity modeling requires taking into account their joint effect.

A. Radar

Typical radar processing, including matched filtering, is very effective in rejecting noise and thus even very weak targets can be found [9]. However, this also means that even weak nonlinear distortion and I/Q mismatch stemming from the non-ideal receiver components may become visible [3]. Therefore, even without any blocker signals, the radar performance may be compromised only due to its own receiver impairments.

For example, in a pulse-Doppler radar employing DCR, the receiver nonlinearities and I/Q mismatch cause false targets which are difficult to distinct from the real targets [10]. More specifically, I/Q mismatch causes mirror-frequency interference (MFI) appearing as a false target for each real target with the same velocity but opposite sign. Similarly, for instance, third-order nonlinearity causes false targets with opposite triple velocity.

B. Communications and Spectrum Sensing

In a communications receiver, the RF/analog hardware nonidealities can cause several problems. This is especially true in a wideband receiver aiming for digitization of several frequency channels or bands with signals having differing power levels, which is exactly the case, e.g., in a multi-carrier receiver digitizing signals simultaneously from multiple transmitters. The transmitter locations, transmission powers and channel fading can result in a scenario where separate carriers have tens of dB's difference in power levels [5]. The strong carriers might drive the analog receiver hardware into nonlinear operation, which creates distortion also outside the transmission bands of the strong carriers. Examples of this distortion are intermodulation distortion (IMD) around the original carrier, harmonic distortion and MFI induced by the I/Q mismatches. This distortion is usually of relatively low level compared to the strong carriers themselves. For example, in [6], $40\,\mathrm{dB}$ spurious-free dynamic range was observed without any post-processing. However, if there is also a substantially weaker signal present at the overall reception band, this signal might be totally masked by either the nonlinear distortion or by MFI. This effectively limits wideband spectrum access and alleviating the problem allows new opportunities in exploiting the available spectrum in more efficient and flexible manner [11].

The spurious components created by the nonlinearities and I/Q mismatches hinder also spectrum sensing for electromagnetic reconnaissance or identification of frequency bands available for opportunistic spectrum access. Concretely, even if a certain frequency band is vacant, the sensing receiver nonlinear distortion may cause the sensing algorithm to falsely claim the band to be occupied. In this scenario removing the distortion, e.g., with the means of digital post-processing allows more reliable sensing [12]. Furthermore, if the sensing is based on certain feature of the detected signal, distortion without this feature might mask the original transmission. This is known as missed detection, the risk of which should be minimized especially in emerging dynamic spectrum access systems in order to avoid interrupting the primary user transmissions [12].

III. Proposed Full-Band Adaptive Interference Cancellation for Wideband Linearization

Herein, the operation principle of the proposed FB-AIC is described and combined with circularity restoring MFI cancellation. The MFI cancellation is performed first for the digitized signal and thus also discussed here shortly before the proposed FB-AIC.

A. Essential Receiver Front-End Modeling

In this paper, a parallel Hammerstein nonlinearity modeling for the receiver front-end is applied. In addition, the RF and BB nonlinearities are modeled in cascade, taking also possible I/Q mismatches into account. Also I/Q mismatch in the down-converting mixer is considered.

A discrete-time baseband equivalent model for the low-noise amplifier (LNA) output is

$$y(n) = a_1(n) * x(n) + a_2(n) * |x(n)|^2 x(n), \tag{1}$$

where $a_1(n)$ and $a_2(n)$ are impulse responses for each polynomial order taking memory effects into account and $x(n)$ is the LNA input. For simplicity, only third-order nonlinear distortion is assumed above. This is also justified because third-order distortion is always the most dominant one [6], [7]. Now, this signal is used as an input for the I/Q mixers, BB amplifiers, and analog-to-digital converters (ADCs). Thereafter, the observed digitized waveform is

$$\begin{aligned} y_{\mathrm{BB}}(n) = {} & b_1(n) * y(n) + b_2(n) * y^*(n) \\ & + b_3(n) * y^3(n) + b_4(n) * [y^*(n)]^3 \\ & + b_5(n) * y^2(n) y^*(n) + b_6(n) * y(n) [y^*(n)]^2, \end{aligned} \tag{2}$$

where $b_1(n)$, $b_2(n)$, $\ldots$, $b_6(n)$ denote the impulse responses for the respective components. These general impulse responses have contribution from the modeled mixer and BB error sources. A detailed description of these contributions can be found from [6]. Also in (2), only third-order nonlinearities are considered in the parallel I/Q chains, together with the I/Q mismatches of the mixers and the BB components. Notice, however, that even though the individual component modeling

TABLE I
TERMS GENERATED BY THE CASCADED NONLINEARITY MODEL

Terms	Conjugate Terms	Interpretation
$x(n)$	$x^*(n)$	Original undistorted signal
$\|x(n)\|^2x(n)$	$\|x(n)\|^2x^*(n)$	3rd-order IMD
$[x^*(n)]^3$	$x^3(n)$	3rd-order harmonics
$\|x(n)\|^4x(n)$	$\|x(n)\|^4x^*(n)$	5th-order IMD
$\|x(n)\|^2[x^*(n)]^3$	$\|x(n)\|^2x^3(n)$	IMD of 3rd-order harmonics (5th order)
$\|x(n)\|^6x(n)$	$\|x(n)\|^6x^*(n)$	7th-order IMD
$\|x(n)\|^4[x^*(n)]^3$	$\|x(n)\|^4x^3(n)$	IMD of 3rd-order harmonics (7th order)
$\|x(n)\|^8x(n)$	$\|x(n)\|^8x^*(n)$	9th-order IMD
$\|x(n)\|^6[x^*(n)]^3$	$\|x(n)\|^6x^3(n)$	IMD of 3rd-order harmonics (9th order)

is based on third-order nonlinear models, the cascaded model of already two such stages yields nonlinear distortion products up to order nine.

When substituting (1) to (2), the cascaded model produces nine separate terms and, if any I/Q mismatch occurs, nine additional conjugate terms. All these terms are shown in Table I. The most essential distortion terms are used as a basis for the cascaded MFI and nonlinearity cancellation discussed in the following subsections. First, the MFI is cancelled from the digitized signal $y_{\text{BB}}(n)$ and thereafter the resulting signal is fed to the linearization stage. This flow is illustrated in Fig. 2.

B. Mirror-Frequency Interference Cancellation

The MFI induced by the I/Q mismatches of the receiver hardware is compensated here in a separate stage, before the linearization processing, whereas in [6] it was performed together with the nonlinearity cancellation. This is illustrated in Fig. 2 with a block diagram showing the separate stages. In practice, the target is to cancel the conjugate terms listed in Table I, the conjugates of the original signal and third-order terms being the most crucial. The MFI cancellation is based on the circularity restoring algorithm discussed in [13], [14]. This earlier algorithm, when it comes to blind parameter learning, is here augmented with a highpass notch filter for removing DC and low frequency content from the received signal which could bias the circularity restoring adaptation. This is essential especially in the scenarios where a baseband signal with DC content is received. Such notch filter aided circularity restoration is also considered in [10]. After finding the cancellation coefficient(s) in this way, the original unfiltered signal is processed in the actual cancellation. This is essential in the aforementioned scenario where the notch filter stopband can also contain desired information. The circularity restoring algorithm has more robust performance compared to the MFI cancellation in [6] also in certain special scenarios, such as in case of frequency symmetric blocker carriers, which are challenging for the error-power minimization based least-mean square (LMS) adaptation used in [6].

The sample-wise adaptation for learning the MFI cancellation parameters is performed as follows. First, the M_1-tap adaptive filter (AF) vector, $\mathbf{w}_{\text{IQ}}$, is initialized as

$$\mathbf{w}_{\text{IQ}}(0) = \mathbf{0}_{M_1\times 1}. \tag{3}$$

Thereafter, the coefficient vector update is formulated as

$$\mathbf{w}_{\text{IQ}}(n+1) = \mathbf{w}_{\text{IQ}}(n) - \lambda\tilde{\mathbf{x}}_{\text{IQ,notch}}(n)\tilde{x}_{\text{IQ,notch}}(n), \tag{4}$$

where λ is the adaptation step-size, $\tilde{\mathbf{x}}_{\text{IQ,notch}}(n) = [\tilde{x}_{\text{IQ,notch}}(n), \tilde{x}_{\text{IQ,notch}}(n-1), \ldots, \tilde{x}_{\text{IQ,notch}}(n-M_1+1)]^{\text{T}}$, being an M_1-sample vector of the adaptation error signal $\tilde{x}_{\text{IQ,notch}}(n) = y_{\text{BB,notch}}(n) + \mathbf{w}_{\text{IQ}}(n)^{\text{T}}\mathbf{y}^*_{\text{BB,notch}}(n)$. The sample vector of the notch-filtered received signal is defined as $\mathbf{y}_{\text{BB,notch}}(n) = [y_{\text{BB,notch}}(n), y_{\text{BB,notch}}(n-1), \ldots, y_{\text{BB,notch}}(n-M_1+1)]^{\text{T}}$. With these AF coefficients $\mathbf{w}_{\text{IQ}}(n)$, the actual MFI cancellation is performed as

$$\tilde{x}_{\text{IQ}}(n) = y_{\text{BB}}(n) + \mathbf{w}_{\text{IQ}}(n)^{\text{T}}\mathbf{y}^*_{\text{BB}}(n), \tag{5}$$

using the original received signal $y_{\text{BB}}(n)$ and an M_1-sample conjugate vector $\mathbf{y}^*_{\text{BB}}(n) = [y^*_{\text{BB}}(n), y^*_{\text{BB}}(n-1), \ldots, y^*_{\text{BB}}(n-M_1+1)]^{\text{T}}$ as in [13].

Now, assuming effective MFI cancellation with the described processing, the I/Q corrected signal $\tilde{x}_{\text{IQ}}(n)$ is fed to the linearization stage, as shown in Fig. 2. The linearization processing aims at cancelling the remaining essential distortion terms in Table I. A novel solution for the full-band linearization is proposed next in the following subsection.

C. Nonlinearity Cancellation

The nonlinearity cancellation stage of the proposed FB-AIC employs a feed-forward structure as illustrated in Fig. 2. The basic principle is to digitally generate an estimate of the nonlinear distortion occurring in the receiver and then subtract the estimate from the I/Q corrected received signal $\tilde{x}_{\text{IQ}}(n)$. This produces then the final linearized signal $\tilde{x}(n)$. The most essential aspect here is thus obtaining accurate estimates of the most prominent nonlinear distortion terms. It can be done by first picking the strongest carrier(s) from $\tilde{x}_{\text{IQ}}(n)$ with bandpass filter(s), producing $\hat{x}_{\text{IQ}}(n)$. In blocker scenarios, this means picking the strongest blocker carriers entering the receiver. If the received signal contains only a single carrier, such as in the radar scenario considered in this paper, this carrier is the one to be bandpass filtered. After that, $\hat{x}_{\text{IQ}}(n)$ is fed through different reference nonlinearities in parallel to produce similar nonlinear distortion products as in the received signal. The exact amount and the structures of the reference nonlinearities required for linearization depend on the characteristics of the analog receiver hardware. In practice, the terms in Table I are good choices for reference nonlinearities, as they directly stem from the complete nonlinear behavioral model of the overall analog receiver chain. Typically it is enough to use a few lowest-order terms (third- and fifth-order) which are typically the strongest [6]. However, these reference nonlinearities do not directly produce a distortion estimate that would exactly match with the received signal distortion. More specifically, the distortion estimate has to be scaled properly and typically also take memory effects into account. Both can be achieved

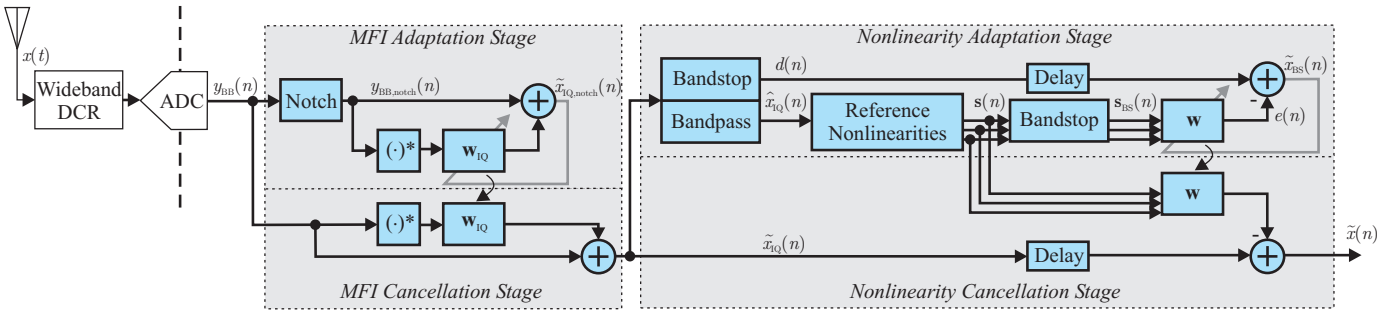

Fig. 2. Block diagram illustrating the principle of the proposed FB-AIC method for receiver I/Q correction and linearization. The MFI and nonlinearity cancellation stages are cascaded and both stages consist of parallel adaptation and cancellation components.

with the AFs, one per considered nonlinear distortion term. Adaptation of the AFs is illustrated in Fig. 2 and also described mathematically later in this subsection. The bandstop filters, shown in Fig. 2, are required in order to guarantee proper convergence of AFs. In practice, the bandstop filter(s) should attenuate the strongest blocker band(s). This means that the signal $d(n)$ (see Fig. 2) is the I/Q corrected signal, including nonlinear receiver distortion, but without the strongest carrier(s).

The essential difference between the nonlinearity cancellation with FB-AIC proposed here and the original AIC described in [6] is related to how the distortion cancellation itself is performed. The adaptation of AFs is similar in both, but the original AIC directly considers $\tilde{x}_{\text{BS}}(n)$, shown in Fig. 2, as the linearized signal. However, the bandstop filters needed for stable coefficient adaptation prevent cancellation of the inband nonlinear distortion on the blocker bands as well as on the bandstop filter transition bands. Especially the limited transition band cancellation performance can be crucial in scenarios where a weak desired carrier is situated on exactly the neighboring band of the blocker carrier. The phenomenon is most pronounced when using limited-order filters, which is usually the case in true implemented hardware. In addition, cancellation of inband distortion when only a single carrier is received, e.g., as in radar receivers, is not possible with the AIC.

In this paper, the above described limitations in linearization performance and flexibility are overcome by performing the coefficient adaptation and the actual nonlinearity cancellation separately, in parallel, as shown in the latter part of Fig. 2. Basically, the bandstop filtering is used when finding and learning the cancellation coefficients, similarly as described in [6]. However, the actual nonlinearity cancellation is performed by using the unfiltered distortion estimates. In this way, the distortion estimates also on the bandstop filter stopbands are maintained and can be used to cancel distortion from the whole received frequency band. In Fig. 2, three parallel distortion estimate lines are drawn as an example but the actual number of the applied estimates can differ from this.

Formally, the nonlinearity cancellation in the proposed FB-AIC is performed so that

$$\tilde{x}(n) = \tilde{x}_{\text{IQ}}(n) - \mathbf{w}^{\text{H}}(n)\mathbf{s}(n), \tag{6}$$

where $\tilde{x}(n)$ is the linearized signal, $\mathbf{w}(n)$ contains the impulse responses of the AFs, and $\mathbf{s}(n)$ contains samples of the considered reference nonlinear transformations without bandstop filtering. More specifically, samples of P reference nonlinearities are stacked into a single vector

$$\mathbf{s}(n) = [\mathbf{s}_1(n), \mathbf{s}_2(n), \ldots, \mathbf{s}_P(n)]^{\text{T}}. \tag{7}$$

For example, stemming from Table I, if the first distortion estimate in $\mathbf{s}(n)$ models the third-order harmonics, then $\mathbf{s}_1(n) = \left[[\hat{x}^*_{\text{IQ}}(n)]^3, [\hat{x}^*_{\text{IQ}}(n-1)]^3, \ldots, [\hat{x}^*_{\text{IQ}}(n-M_2+1)]^3\right]^{\text{T}}$, where M_2 is the AF length. The other $P-1$ reference signals are obtained accordingly, using the selected reference nonlinearities from Table I.

The LMS adaptation for the parameter learning can be formulated mathematically when denoting the bandstop filtered distortion estimates as

$$\mathbf{s}_{\text{BS}}(n) = [\mathbf{s}_{\text{BS},1}(n), \mathbf{s}_{\text{BS},2}(n), \ldots, \mathbf{s}_{\text{BS},P}(n)]^{\text{T}}. \tag{8}$$

It is worth noting that the only difference between (7) and (8) is the bandstop filtering. Also the AF coefficients are gathered into a single vector

$$\mathbf{w}(n) = [\mathbf{w}_1(n), \mathbf{w}_2(n), \ldots, \mathbf{w}_P(n)]^{\text{T}}. \tag{9}$$

For the adaptation, first, the AF vector $\mathbf{w}$ is initialized as

$$\mathbf{w}(0) = \mathbf{0}_{PM_2\times 1}, \tag{10}$$

if no *a priori* information is available. Thereafter, the combined AF output for $n = 0, 1, 2, \ldots$ is

$$e(n) = \mathbf{w}^{\text{H}}(n)\mathbf{s}_{\text{BS}}(n). \tag{11}$$

This results in the adaption error

$$\tilde{x}_{\text{BS}}(n) = d(n) - e(n) \tag{12}$$

and finally the AF update is given by

$$\mathbf{w}(n+1) = \mathbf{w}(n) + \text{diag}(\boldsymbol{\mu})\tilde{x}^*_{\text{BS}}(n)\mathbf{s}_{\text{BS}}(n), \tag{13}$$

where $\text{diag}(\cdot)$ denotes a function for converting a vector to a diagonal matrix. The overall step-size vector $\boldsymbol{\mu}$ contains different step sizes for every distortion branch with M_2 steps per branch, thus $\boldsymbol{\mu}$ is a $PM_2 \times 1$ vector. For increased adaptation stability, normalized least-mean square (NLMS)

TABLE II
SIMULATED RECEIVER PARAMETERS

Parameter	Value
LNA gain	20 dB
LNA IIP3	0 dBm
Mixer IRR	30 dB
Baseband gain	20 dB
Baseband IIP3	20 dBm
Sampling rate	40 MHz
Effective RX bandwidth	30 MHz
Quantization	14 bits

should be used. This adds PM_2 scaling coefficients, one for each of the step sizes in $\boldsymbol{\mu}$ and is documented in [6]. In FB-AIC, these AF coefficients $\mathbf{w}$ are used in the actual linearization as described in (6). Due to the parallel adaptation and nonlinearity cancellation, the AFs can be adapted all the time during the receiver operation or it is also possible, after initial convergence, to update the AFs less frequently to save computations.

IV. SIMULATED AND MEASURED LINEARIZATION PERFORMANCE

Herein, the performance of the proposed FB-AIC is illustrated in two separate scenarios. The first one is a radar receiver suffering from nonlinear distortion and MFI. In the latter one, a multi-carrier communications receiver with similar non-idealities is considered. In radar scenario, the main emphasis is on cancelling the inband self-distortion of the received radar waveform. In the communications scenario, cancelling also out-of-band distortion stemming from the strong carriers has a significant role because the distortion is potentially falling on top of desired weaker carriers.

Similar receiver characteristics are simulated in both scenarios. These parameters are summarized in Table II. The nonlinear characteristics of the RF and BB gain stages result in balanced distortion profile where neither of the stages alone acts as a linearity bottleneck. The nonlinearities are modeled as third-order polynomials per stage, resulting in ninth-order overall distortion profile, as elaborated in the previous section.

AIC [6] and FB-AIC implementations employ NLMS adaptation and cancellation of third-order intermodulation and harmonic distortions is targeted. The MFI is cancelled by the circularity restoring principle in case of FB-AIC. In the AIC processing, the mirror components of the original signal, third-order intermodulation and third-order harmonic distortions are included in the nonlinearity modeling. Following the introduced notation, the number of distortion estimates $P = 2$ and the used reference nonlinearities, stemming from Table I, are of the form $s_1(n) = |\hat{x}_{\mathrm{IQ}}(n)|^2 \hat{x}_{\mathrm{IQ}}(n)$ and $s_2(n) = [\hat{x}^*_{\mathrm{IQ}}(n)]^3$. In the actual LMS adaptation, the samples of these reference nonlinearities are stacked into $\mathbf{s_1}(n)$ and $\mathbf{s_2}(n)$ vectors, as described in (7).

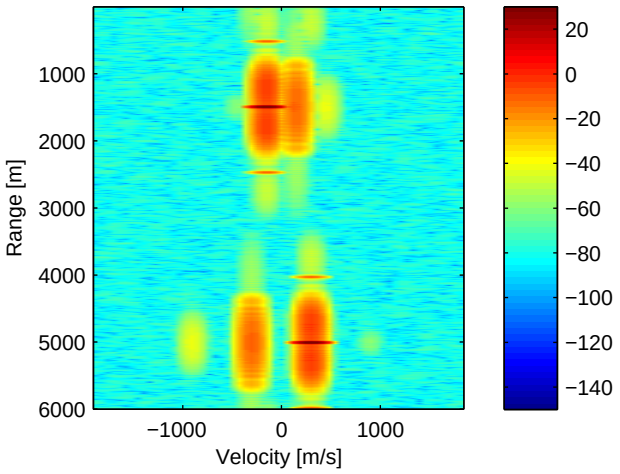

Fig. 3. Range-Doppler matrix before linearization. The colors denote observed power at different ranges and velocities on logarithmic scale. MFI is clearly visible at opposite velocities and third-order nonlinearity at three times the opposite velocities.

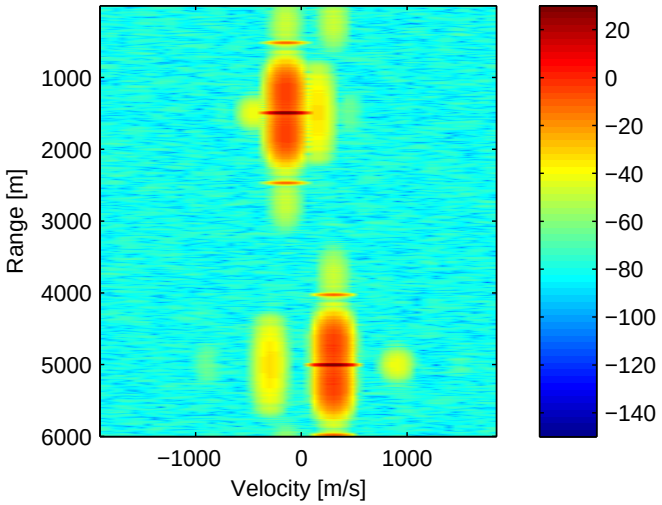

Fig. 4. Range-Doppler matrix after linearization. The colors denote observed power at different ranges and velocities on logarithmic scale. MFI and third-order nonlinearity levels are clearly suppressed compared to Fig. 3.

A. Radar Simulations

In the radar scenario, a pulsed $10\,\mathrm{MHz}$ linear frequency modulation (LFM) signal is studied, giving effective oversampling ratio of 3 inside the reception band of $30\,\mathrm{MHz}$. This oversampling allows observing also the out-of-band intermodulation which is exploited in the adaptation process. The width of a single pulse is $5\,\mu\mathrm{s}$ and pulse repetition frequency is $25\,\mathrm{kHz}$. Two targets with ranges of $1500\,\mathrm{m}$ and $5000\,\mathrm{m}$ are observed. The target velocities are $-150\,\mathrm{m/s}$ and $300\,\mathrm{m/s}$.

The range-Doppler matrices before and after the linearization processing are shown in Fig. 3 and Fig. 4, respectively. The average receiver input power in this scenario is $-27\,\mathrm{dBm}$. When comparing the figures, it is clear that the MFI is reduced, pushing down the false target having opposite velocity. At the same time, also the opposite triple velocity false target is

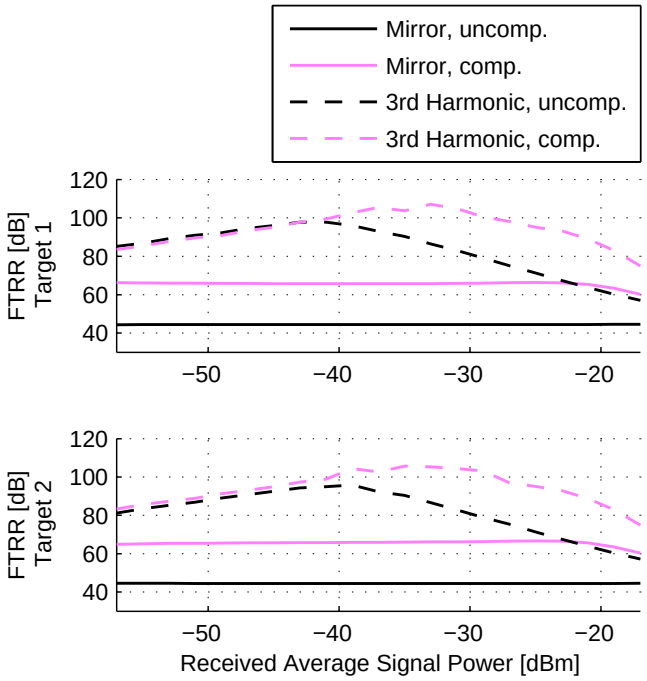

Fig. 5. The FTRR results for both targets as a function of the received average signal power before ("uncomp.") and after ("comp.") the linearization. The mirror target created by the MFI and the triple mirror target created by the nonlinearities are considered.

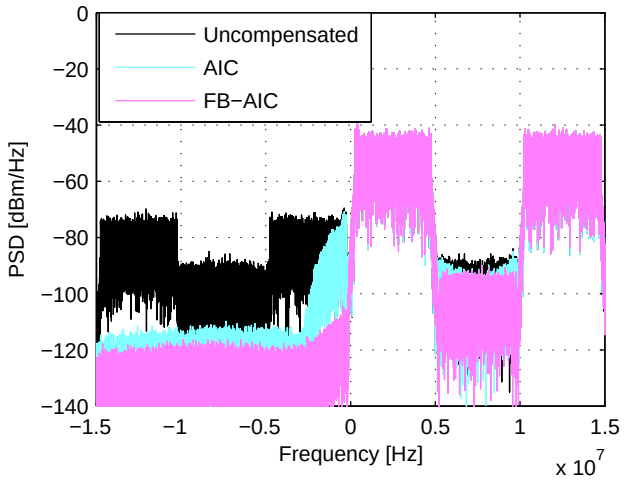

Fig. 6. The spectra of the uncompensated and compensated signals illustrating the improved performance of the FB-AIC compared to AIC. The blocker RF input powers are $-27\,\mathrm{dBm}$ and weak carrier power is $-77\,\mathrm{dBm}$.

reduced by the nonlinearity cancellation, which is pushing the third harmonic down.

The false target cancellation performance is further studied with a signal power sweep, for which the false target rejection ratios (FTRRs) are calculated for the opposite velocity (mirror) target and the opposite triple velocity (3rd harmonic) target. The FTRR is defined mathematically as

$$FTRR[\mathrm{dB}] = 10\log_{10}\frac{P_{\mathrm{true}}}{P_{\mathrm{false}}}, \tag{14}$$

where P_{true} and P_{false} denote the observed powers for true and false targets, respectively. The results are illustrated in Fig. 5. This shows that for both the targets, the mirror target level is suppressed by more than $20\,\mathrm{dB}$. At the same time, with high reception powers, above $-40\,\mathrm{dBm}$, the false target appearing because of the third harmonic is also suppressed. With FB-AIC, e.g., $80\,\mathrm{dB}$ FTRR can be maintained with $11\,\mathrm{dB}$ higher reception powers than without FB-AIC.

B. Communications Simulations

In the communications scenario, reception of a weak carrier in the presence of neighboring band blocking carriers is studied. An example spectrum of the composite waveform is shown in Fig. 6. The three orthogonal frequency-division multiplexing (OFDM) modulated carriers, with 16-QAM subcarrier modulation, have $5\,\mathrm{MHz}$ nominal bandwidth and center frequency separation while $4.5\,\mathrm{MHz}$ per carrier is employed for data transfer, resulting in symmetric $250\,\mathrm{kHz}$ carrier-wise guard bands. After the I/Q downconversion from RF to intermediate frequencies, the remaining center frequencies of the blocking carriers are $2.5\,\mathrm{MHz}$ and $12.5\,\mathrm{MHz}$, the weak carrier being centered at $7.5\,\mathrm{MHz}$.

In Fig. 6, it is also clearly visible that the original AIC has limited distortion cancellation performance on the neighboring bands of the blockers. This is because of the wide transition bands of the 100-tap bandpass and bandstop filters used in the adaptation process. The stopband attenuations of these filters are set to $60\,\mathrm{dB}$ while passband ripple of $0.1\,\mathrm{dB}$ is allowed. Furthermore, in Fig. 6, it is evident that this limitation is greatly alleviated when applying the FB-AIC processing.

This improvement in the linearization performance is further illustrated in Fig. 7 and Fig. 8, showing the distortion rejection ratio (DRR) and symbol error ratio (SER) of the weak carrier, respectively. Herein, the DRR is defined as

$$DRR[\mathrm{dB}] = 10\log_{10}\frac{S+N}{D}, \tag{15}$$

where S, N, and D are signal, noise, and distortion powers, respectively. In Fig. 7, the AIC [6] gives DRR improvement of few dB's over the whole blocker power range compared to the uncompensated scenario. At the same time, the proposed FB-AIC is able to improve the DRR significantly, allowing 8 dB improvement in the blocker tolerance at $20\,\mathrm{dB}$ DRR level. Fig. 7 gives also the weak signal's signal-to-noise ratio (SNR) for reference. In practice, the DRR values above the SNR level mean that the distortion is already pushed below the noise floor and therefore further increase in DRR is typically not beneficial. Furthermore, similar performance improvement is visible also in Fig. 8, where FB-AIC helps to maintain, e.g., $1\,\%$ SER level with $8\,\mathrm{dB}$ higher blocker power levels.

Furthermore, the performance of the AIC and FB-AIC is compared in Fig. 9 with input-output characteristic plots. In the uncompensated scenario, saturating nonlinear behavior is visible. It should be noted that even if the saturating behavior is mild for the overall waveform, it still creates significant

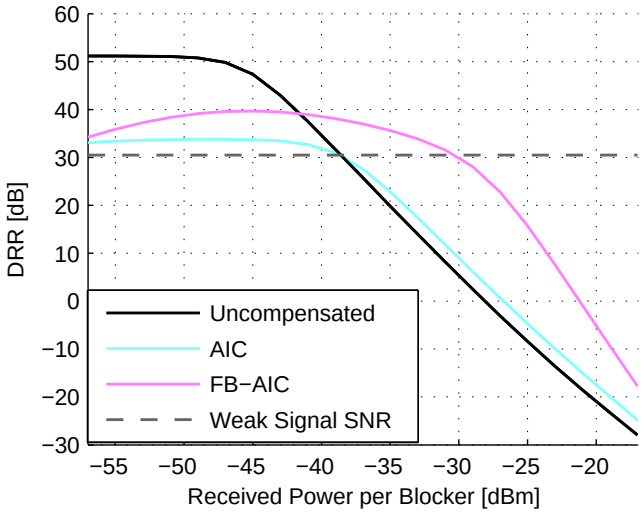

Fig. 7. The DRR of the weak desired carrier between the blocking carriers before compensation and after AIC and FB-AIC as a function of the received blocker power in RF input. The weak carrier power is constant $-77\,\mathrm{dBm}$.

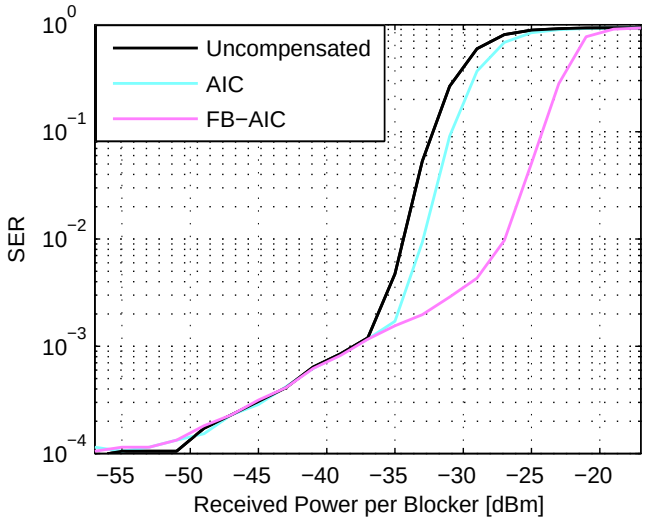

Fig. 8. The simulated SER of the 16-QAM subcarrier-modulated weak OFDM carrier between the blocking carriers before compensation and after AIC and FB-AIC. The weak carrier power is constant $-77\,\mathrm{dBm}$.

distortion on the weak signal band, as shown above. Based on the DRR and SER results this is to some extent alleviated with the AIC, shown in the middle, but nonlinear curve is still visible, illustrated by the data-fitted third-order curve. In parallel, the rightmost plot with the FB-AIC processed data shows basically linear behavior. The performance difference is well illustrated here because the overall nonlinear distortion in the composite signal has the highest levels on the blocker bands, even though, because of the high signal power, the blockers retain good relatively DRR. Because the FB-AIC is able to cancel also the distortion on the blocker bands, it is able to linearize the overall waveform significantly.

C. Measured Performance

The linearization performance of AIC and FB-AIC is compared with true measured RF signals in Fig. 10. The measured three-carrier OFDM scenario is similar to the simulated scenario of the previous subsection. The RF center frequency in the measurements is $1750\,\mathrm{MHz}$. For signal generation National Instruments PXIe-5645R vector signal transceiver has been employed [15]. The main nonlinearity source is a HD Communications Cor. HD24089 LNA [16]. A state-of-the-art RX board is used for signal down-conversion and data aquisition. This setup essentially represents a typical radio receiver scenario where the LNA is the dominating nonlinearity source. In Fig. 10, IMD spread around the original carriers is observed, masking the weak carrier. In addition, the MFI induced by the down-converting mixers and the RX baseband is seen. However, it is evident that FB-AIC has improved performance in close proximity of the blockers, also in this RF measurement scenario. As a concrete example, the SER of the weak 16-QAM modulated signal is presented in Fig. 10 before and after compensation showing about 8 dB of improvement in blocker tolerance at 1 % SER level with the FB-AIC. The compensation performance of the AIC is again quite limited as can be seen.

V. Conclusion

A fully digital wideband receiver nonlinearity cancellation method was proposed. Compared to the state-of-the art, the proposed method has improved performance on the bands of the strongest distortion producing carriers, i.e., blockers, and their neighboring bands. This improvement was verified in two applications, namely radar and multi-carrier communications reception. The radar scenario concentrated on the inband distortion cancellation, whereas in the communication scenario, the neighboring band performance was illustrated with realistic filter orders in the processing. Furthermore, the performance of the proposed method was illustrated also with preliminary RF hardware measurements. More extensive measurements will be provided in the final version of the paper. In general, improved flexibility in analog receiver hardware design and wideband spectrum access can be achieved with the proposed digital nonlinearity cancellation method.

References

[1] A. A. Abidi, "Direct-conversion radio transceivers for digital communications," *IEEE J. Solid-State Circuits*, vol. 30, no. 12, pp. 1399–1410, Dec. 1995.

[2] B. Razavi, "Design considerations for direct-conversion receivers," *IEEE Trans. Circuits Syst. II*, vol. 44, no. 6, pp. 428–435, June 1997.

[3] G. Vallant, M. Allén, S. Singh, M. Epp, S. Chartier, and M. Valkama, "Direct downconversion architecture performance in compact pulse-doppler phased array radar receivers," in *Proc. IEEE 13th Topical Meeting on Silicon Monolithic Integrated Circuits in RF Systems*, Austin, TX, USA, Jan. 2013, pp. 102–104.

[4] D. H. Mahrof, E. A. M. Klumperink, J. C. Haartsen, and B. Nauta, "On the effect of spectral location of interferers on linearity requirements for wideband cognitive radio receivers," in *Proc. IEEE Symp. on New Frontiers in Dynamic Spectrum*, Singapore, Apr. 2010, pp. 1–9.

[5] B. Razavi, "Cognitive radio design challenges and techniques," *IEEE J. Solid-State Circuits*, vol. 45, no. 8, pp. 1542–1553, Aug. 2010.

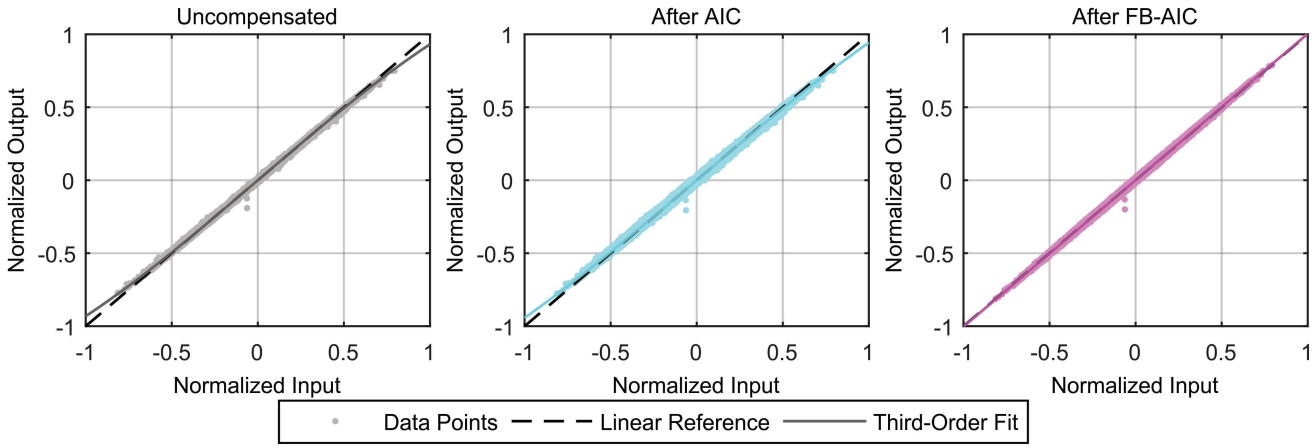

Fig. 9. Input-output characteristics of the composite communications waveform with blocker RF input powers of $-27\,\mathrm{dBm}$. The uncompensated (left) characteristics are shown together with AIC (middle) and FB-AIC (right) compensated plots.

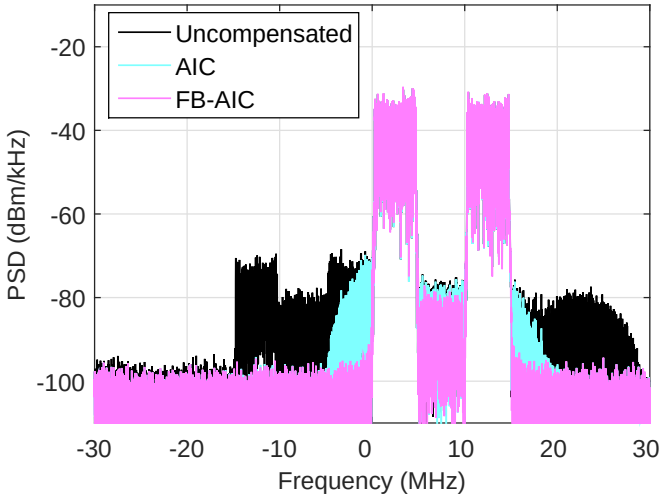

Fig. 10. A comparison of the AIC and FB-AIC in laboratory RF measurements. The blocker powers in presented scenario at receiver input are $-25\,\mathrm{dBm}$ and the weak signal power is $-72\,\mathrm{dBm}$. The RF frequency range in the measurements is $700\,\mathrm{MHz}$.

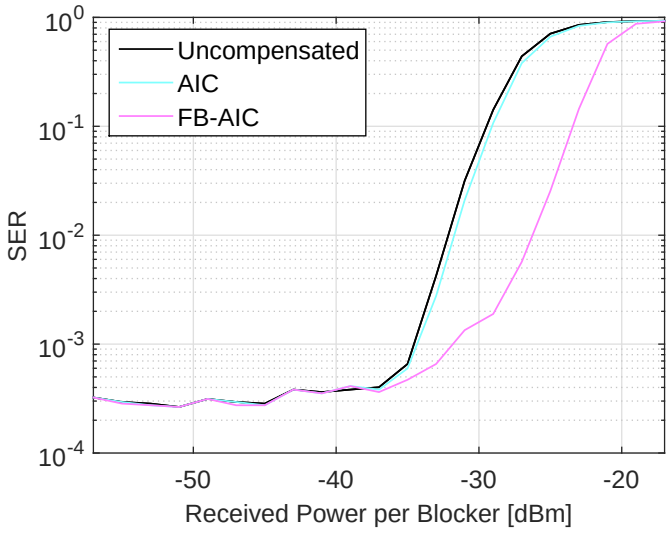

Fig. 11. The measured SER of the 16-QAM subcarrier-modulated weak OFDM carrier between the blocking carriers before compensation and after AIC and FB-AIC. The weak carrier power is constant $-72\,\mathrm{dBm}$.

[6] M. Grimm, M. Allén, J. Marttila, M. Valkama, and R. Thomä, "Joint mitigation of nonlinear RF and baseband distortions in wideband direct-conversion receivers," *IEEE Trans. Microw. Theory Tech.*, vol. 62, no. 1, pp. 166–182, Jan. 2014.

[7] E. Keehr and A. Hajimiri, "Equalization of third-order intermodulation products in wideband direct conversion receivers," *IEEE J. Solid-State Circuits*, vol. 43, no. 12, pp. 2853–2867, Dec. 2008.

[8] ——, "Successive regeneration and adaptive cancellation of higher order intermodulation products in RF receivers," *IEEE Trans. Microw. Theory Tech.*, vol. 59, no. 5, pp. 1379–1396, May 2011.

[9] M. A. Richards, J. A. Scheer, and W. A. Holm, Eds., *Principles of Modern Radar: Basic Principles*. Raleigh, NC: SciTech Publishing, 2010.

[10] G. Vallant, M. Epp, W. Schlecker, U. Schneider, L. Anttila, and M. Valkama, "Analog IQ impairments in zero-IF radar receivers: Analysis, measurements and digital compensation," in *Proc. IEEE Int. Instrumentation and Measurement Technology Conf.*, Graz, Austria, May 2012, pp. 1703–1707.

[11] M. Allén, J. Marttila, M. Valkama, M. Grimm, and R. Thomä, "Digital post-processing based wideband receiver linearization for enhanced spectrum sensing and access," in *Proc. 9th Int. Conf. Cognitive Radio Oriented Wireless Networks and Commun.*, June 2014, pp. 520–525.

[12] M. Allén, J. Marttila, M. Valkama, S. Mäkinen, M. Kosunen, and J. Ryynänen, "Digital linearization of direct-conversion spectrum sensing receiver," in *Proc. 1st IEEE Global Conf. Signal and Information Process.*, Austin, TX, USA, Dec. 2013, pp. 1158–1161.

[13] L. Anttila, M. Valkama, and M. Renfors, "Circularity based I/Q imbalance compensation in wideband direct-conversion receivers," *IEEE Trans. Veh. Technol.*, vol. 57, no. 4, pp. 2099–2113, July 2008.

[14] L. Anttila, "Digital front-end signal processing with widely-linear signal models in radio devices," Ph.D. dissertation, Tampere University of Technology, Finland, 2011.

[15] National Instruments. NI PXIe-5644R/5645R/5646R 6 GHz RF vector signal transceivers. [Online]. Available: http://www.ni.com/datasheet/pdf/en/ds-422

[16] HD Communications Corp. Low noise amplifier HD24089. [Online]. Available: http://www.rfcomp.com/download/product_specs/low_noise/HD24089specs.pdf